

Submitted: 2008 June 13; accepted: 2008 — —

Spitzer 24 μm detections of starburst galaxies in Abell 851

Alan Dressler, Jane Rigby, & Augustus Oemler Jr.

*The Observatories of the Carnegie Institution of Washington, 813 Santa Barbara St.,
Pasadena, California 91101-1292*

dressler@ociw.edu, jrigby@ociw.edu, & oemler@ociw.edu

Jacopo Fritz & Bianca M. Poggianti

INAF-Osservatorio Astronomico di Padova

Osservatorio Astronomico di Padova, vicolo dell'Osservatorio 5, 35122 Padova, Italy

bianca.poggianti@oapd.inaf.it & jacopo.fritz@gmail.com

George Rieke & Lei Bai

Steward Observatory, University of Arizona, Tucson, AZ 85721

grieke@as.arizona.edu & bail@as.arizona.edu,

ABSTRACT

Spitzer-MIPS 24 μm observations and ground-based optical imaging and spectroscopy of the rich galaxy cluster Abell 851 at $z = 0.41$ are used to derive and compare star formation rates from the mid-IR 24 μm and from [O II] $\lambda\lambda 3727$ emission. Many cluster galaxies have $\text{SFR}(24 \mu\text{m}) / \text{SFR}([\text{O II}]) \gg 1$, indicative of star formation in regions highly obscured by dust. We focus on the substantial minority of A851 cluster members where strong Balmer absorption points to a starburst on a 10^{8-9} year timescale. As is typical, two types of galaxies with strong Balmer absorption are found in A851: with optical emission (starforming), and without (post-starburst). Our principal result is that the starforming variety, so-called e(a) galaxies, are mostly detected (9 out of 12) at 24 μm — for these we find typically $\text{SFR}(24 \mu\text{m}) / \text{SFR}([\text{O II}]) \sim 4$. Strong Balmer absorption and high values of $\text{SFR}(24 \mu\text{m}) / \text{SFR}([\text{O II}])$ indicate moderately active starbursts; both observations support the picture that e(a) galaxies are the

active starbursts that feed the post-starburst population. While $24\ \mu\text{m}$ detections are frequent with Balmer-strong objects (even 6 out of 18 of the supposedly “post-starburst” galaxies are detected), only 2 out of 7 of the continuously star-forming ‘e(c)’ galaxies (with weak Balmer absorption) are detected — for them, $\text{SFR}(24\ \mu\text{m})/\text{SFR}([\text{O II}]) \sim 1$. Their optical spectra resemble present-epoch spirals that dominate today’s universe; we strengthen this association by showing that $\text{SFR}(24\ \mu\text{m})/\text{SFR}([\text{O II}]) \sim 1$ is the norm today. That is, not just the amount of star formation but also its mode has evolved strongly from $z \sim 0.4$ to the present. We fit spectrophotometric models in order to measure the strength and duration of the bursts and to quantify the evolutionary sequence from active- to post-starburst. Our results harden the evidence that moderately active starbursts are the defining feature of starforming cluster galaxies at $z \sim 0.4$.

Subject headings: galaxies: clusters: general – galaxies: evolution

1. Introduction

A remarkable change in our view of galaxy evolution over the last few decades has been the realization that the properties of galaxies are changing on relatively short time scales, in cosmic terms. The Butcher-Oemler (1978) effect, first at-odds with the then-prevailing picture that strong galaxy evolution occurred only within the first few billion years, is now part of the orthodoxy – a large and still-growing body of evidence shows that the stellar populations and even the morphologies of many galaxies have undergone significant change, even within the last 4 billion years. Butcher and Oemler’s discovery of a substantial population of luminous starforming galaxies in intermediate-redshift clusters – a great contrast with cluster populations today where only a small fraction of galaxies are still actively forming stars – is now widely confirmed and accepted.

Less well known, but likely as important for understanding the causes of the Butcher-Oemler effect, is the discovery by Dressler and Gunn (1983) that most of these starforming galaxies in the cores of distant clusters show a starburst signature in their optical spectra: both starbursts and post-starbursts are common. Later work has confirmed the ubiquity of this result (Couch & Sharples 1987, Wirth et al. 1994, Poggianti et al. 1999 – P99, Tran et al. 2003).¹ Data from these studies suggest that a significant fraction of field populations at $z \sim 0.5$ is also undergoing moderate bursts of star formation (Dressler et al. 2004). This

¹Interested readers will appreciate a review of the often-cited rebuttal by Balogh et al. (1999). These authors actually found a 5% incidence of strong Balmer-line sources — for a lower redshift cluster sample,

behavior contrasts with today’s population of field galaxies, for which continuous star forming is the dominant mode, and starbursts are rare. This is yet further evidence of rapid evolution of the galaxy population, at least as important, since it applies to field and cluster galaxies alike.

In this paper we address one of the long-standing uncertainties of this subject — the amount of dust-obscured star formation that has not been generally accounted-for in representative field and cluster populations at $z \sim 0.5$. Although Balmer absorption is a reliable indicator of past starburst activity, a coherent picture requires evidence of the bursts themselves. This has been hampered by the possibility that much of the star formation is obscured by dust, and therefore not part of the tally made with optical-to-near-IR observations. The remarkable sensitivity of the Spitzer Space Telescope with its 24 μm MIPS camera is allowing great progress in removing this uncertainty.

As part of a successful Spitzer program to observe two rich clusters of galaxies, we investigated archival MIPS data for Abell 851, a cluster that is well studied in the optical, x-ray, and radio, and for which a significant spectroscopic sample has been obtained and explored in a companion paper (Oemler et al. 2008, hereinafter Oem08). Our purpose here is limited to the implications for the amount and character of star formation in distant clusters, specifically the subject of “starburst vs. continuously starforming” for distant galaxies. Issues of causes and mechanisms are beyond the scope of this paper, but Spitzer data for additional rich, distant clusters and their surrounding field populations will be able to advance these discussions considerably.

The paper is organized as follows. In section 2 we lay out the issues, in Section 3 we address the ability of mid-infrared imaging to add to our knowledge of the star formation rates of distant galaxies, in Section 4 we present the optical and mid-IR data for A851, and Section 5 we give the results of combining these data sets. In Section 6 we compare our detections of dusty starbursts in A851 with similar observations of present-epoch spirals. Finally, in Section 7, we apply stellar population models to the optical spectra + MIPS data and discuss the results in terms of a consistent picture of the starburst activity in distant clusters.

with a higher threshold of Balmer strength — quite consistent with the other work cited above. Balogh et al. discounted their detections as simple noise in their spectra, after determining the “noise” from the $H\delta$ distribution in their full sample. Dressler et al. (2004) show that the detections were in fact reliable – and the noise greatly overestimated — due to a difficulty with the bandpass measurement technique, which for small $H\delta$ equivalent width returns negative values — see also Prochaska et al. 2007.

2. Where are the starbursts that feed the post-starburst population?

Dressler & Gunn (1983) first reported spectra of L^* galaxies in distant clusters with strong Balmer absorption but no emission lines and interpreted these as *post-starburst* (see also Couch & Sharpes 1987, P99). The question “where are the *active* starbursts that turn into post-starburst galaxies?” was largely set aside. Dressler, Gunn, and Schneider (1985) noted only a few examples in CL0024+24 of nearly pure emission-line spectra — characteristic of today’s strong starbursts, for example, Markarian galaxies. But, because it was expected that the starburst phase would be short, $\tau \lesssim 10^8$ yr, compared to the $\tau \sim 10^9$ yr that the galaxy would be recognized as post-starburst, it was reasonable at first to expect to catch few of the actual starbursts. This explanation became untenable as the Morphs study of 10 clusters accumulated more than 100 post-starburst spectra: although some tens of emission-line-dominated spectra were identified, their distribution was distinctly shifted to lower-luminosities than the post-starburst galaxies — the predecessors to the post starbursts would be, if anything, more luminous (P99).

However, the larger Morphs sample provided an alternate explanation. In addition to the post-starbursts, the Morphs sample included a substantial number of galaxies with strong $H\delta$ **and** (relatively weak) [O II] emission. Initially, these were interpreted as decaying starbursts — a phase of subsiding star formation between the main burst and the post-starburst phase. However, the dusty appearance of many of these ‘e(a)’ galaxies (‘e’ for emission, ‘a’ for A-stars) led P99 to another explanation — that e(a) galaxies were, in fact, the actual starbursts. If heavily obscured by dust, [O II] emission would greatly under-represent the star formation rate. As examples, P99 pointed to the Liu & Kennicutt (1995) sample of present-day mergers, which shared the spectral properties of the e(a) galaxies (see Poggianti & Wu 2000, Poggianti, Bressan, & Franceschini 2001). Liu & Kennicutt showed, from IRAS mid-IR observations and optical imaging, that the majority of star formation in such systems is hidden by dust from optical or near-IR observation. Detection with the VLA of a radio continuum of many of these putative dusty starbursts in the distant cluster sample also supported the idea of hidden star formation (Smail et al. 1999). Furthermore, radio detections of a few supposedly *post-starburst* galaxies suggested that dust might be hiding continuing star formation in some of these as well.

Subsequent work has been supportive of the identification of dusty starbursts in distant clusters. ISOCAM contributed extensively to the study of mid-IR emission from present-epoch galaxies at all types was extensive. In particular, Duc et al. (2002) and Fadda et al. (2002) made pioneering observations of galaxies in clusters at $z \sim 0.2$. ISOCAM’s sensitivity did not allow it to detect typical starforming galaxies at $z \sim 0.5$, and even at $z \sim 0.2$ the detections were mostly luminous infrared galaxies (LIRGs). Despite limited sensitivity,

several studies detected luminous, dusty starbursts in clusters at these redshifts, galaxies that are rare (at best) in rich clusters at $z=0$. The pre-Spitzer era of mid-IR emission from galaxies is well and thoroughly reviewed by Metcalfe et al. (2005).

Now, with MIPS on Spitzer, it is possible to measure star formation rates $\sim 1 M_{\odot} \text{ yr}^{-1}$ at $z \sim 0.5$, a value typical of normal spiral galaxies today. This means that L^* galaxies with even modestly elevated rates of star formation compared to today’s spirals are detectable, allowing us to test directly the claim by the Morphs that the e(a) galaxies in intermediate-redshift clusters are dusty starbursts of sufficient luminosity to feed the post-starburst population and judge, as well, whether the post-starburst galaxies are really **post** starburst.

Ours is not the first study to use MIPS on Spitzer to image intermediate-redshift clusters. Geach et al. (2006) targeted two clusters at $z \sim 0.5$ and found many mid-IR sources in one, although comparatively few in another cluster of similar richness. They describe the properties of the population – luminosity function, spatial distribution, etc., but do not analyze the properties the individual galaxies and basically bypass the question of starbursts, consistent with the paradigm favored by Geach et al. in which starforming galaxies falling into clusters are simply extinguished.

Bai et al. (2007) and Marcillac et al. (2007) imaged two very rich clusters at $z \sim 0.8$, for which they detected 30-plus galaxies in the mid-IR that are either confirmed or suspected (photometric redshift) cluster members. Because of the greater distance relative to the Geach et al. clusters and A851, the detected galaxies have greater rates of star formation — tens of solar masses per year — most of these can be classified as LIRGS. The optical spectra of these mid-IR detections argue that these galaxies are strongly star-forming and considerably obscured by dust. Both Bai et al. and Marcillac et al., like Geach et al., analyze the properties of the population, velocity kinematics, galaxy morphology, spatial distribution, particularly with respect to x-ray emission, colors, and luminosity distribution. In addition, Marcillac et al. investigate the correlation with optical spectral types – passive, starforming, and post-starburst, but their sample included only 4 galaxies that are candidates for active, dusty starbursts, of which 3 are detected in the mid-IR. Our goal in this and subsequent studies is to extend this comparison of optical spectra and mid-IR emission to typical star-forming galaxies of lower luminosities, which will provide a fuller picture of the evolution of the cluster population, $L > 0.4L^*$.

This study of A851 and the future observations we will obtain with Spitzer-MIPS will provide crucial data for understanding the star formation history of galaxies that are involved in building intermediate-redshift clusters. The optical spectroscopy and photometry of such samples are missing information about dust obscuration that is necessary to this task; adding the Spitzer data provides such data. We will pay particular attention to the presence of

Balmer absorption in our sample galaxies, highlighting the importance of starbursts in cluster evolution (see D99, P99 and references therein). Unlike the other studies of clusters with Spitzer-MIPS, we will concentrate on modeling the star formation history with the critical addition of the mid-IR data. Specifically, through basic stellar population models of the data, we will address the question of whether the distinctions we have drawn between continuously starforming, starbursting, and post-starburst galaxies are quantitatively consistent with the observations of intermediate-redshift cluster galaxies.

3. The Data

3.1. Basic properties of the rich cluster of galaxies Abell 851

The rich cluster Abell 851 (aka CL0939+4713) at $z = 0.41$ is one of the best-studied intermediate-redshift clusters and one of the clusters in which post-starburst galaxies were first identified (Dressler & Gunn 1992). A851 is among the most populous clusters known at its epoch and is also noteworthy because it appears to be in the process of assembly through the mergers of several subclusters. This is especially evident in X-ray observations (Schindler et al. 1998) where two prominent centers of emission are also centers of galaxy concentration.

Although A851 is unusually rich and dynamically active, its galaxy population is not qualitatively different from that of other rich clusters at $z \sim 0.5$, as shown by studies by the Morphs collaboration (Smail et al. 1997, Dressler et al. 1999, P99, D04, Oem08). The majority of its galaxies are red, passive elliptical and S0 galaxies, but A851 is also well represented in both types of galaxies with strong Balmer absorption: those without emission that are identified as post-starburst, and those with emission that have been suggested to be dust-obscured, active starbursts that feed the post-starburst population (P99).

Oem08 studied an extended region $R \sim 2 - 3$ Mpc around the core of A851, including HST images and spectroscopy for both an extended square region and the remarkable filament that stretches further, to the north-west of the cluster. Oem08 found a substantial population of active starbursts and fewer post-starburst galaxies in the outskirts of A851, consistent with idea that many of the starbursts are triggered well outside the cluster core, probably within the infalling groups from which the cluster is growing (P99, Treu et al. 2003, Moran et al. 2007). Oem08 also found another population of starbursts that appear to have been triggered by passing through the cluster core.

Oem08 also show that the morphology-density relation for this cluster is well developed, even though it is, at $z = 0.41$, in a unrelaxed dynamical state. From the spatially extended sample it appears that A851 is one of the most active clusters known in terms of star

formation and starbursts, but that these differences are quantitative rather than qualitative, and likely the result of the very dynamic phase in which it is observed. A complete description of A851, the observations, and the implications for galaxy evolution in clusters can be found in Oem08.

3.2. Optical data and Spitzer-MIPS Observations

The optical data for this study includes photometry and spectroscopy from Dressler & Gunn (1992) and the Morphs collaboration. HST WFPC-2 observations that cover a 3x3 mosaic (480 arcsec square) are described in Smail et al. (1997) and Oem08. The morphological information from these images is mainly discussed in Oem08 and briefly referenced here, but these fields basically define the extent of the photometric and spectroscopic sample that we use here. The photometric data come from these HST frames and ground-based observations by Dressler & Gunn. The spectroscopic data come from Dressler & Gunn and the Morphs collaboration (Dressler et al. 1997, D99); they are explained in more detail in Oem08.

The core of Abell 851 was mapped in 24 μm by MIPS in Spitzer GTO program 83 (PI G. Rieke). The background level was 32 MJy/SR, which is classified as “medium” by the SSC. The observation was done in Photometry Mode, with six cycles of half-frame-overlapping coverage, and individual exposure times of 30 s. The resulting exposure time per-pixel is 2685 s in a $5' \times 5'$ box centered on the cluster, and 900 s in two flanking boxes each $5' \times 2.2'$ in area. The online SSC tool SENS-PET estimates that these exposure times should have 5σ point source sensitivities of 70 and 120 μJy , respectively. At these depths, confusion noise from extragalactic sources becomes important.

The 24 μm images were reduced and combined into a mosaic using the Data Analysis Tool (Gordon et al. 2006) with a few additional processing steps (Egami et al. 2006). Photometry at 24 μm was obtained by PSF fitting using the DAOPHOT task *allstar*, as detailed in Rigby et al. (2008).

The areas covered by optical spectroscopy and MIPS 24 micron are of similar size, but not entirely coincident. There are 101 cluster members with high-quality optical spectra ($Q \leq 3$, see Oem08 for more information). Of these, 83 have MIPS 24 μm coverage. Of those, 22 are Spitzer detections with $f(24 \mu\text{m}) > 80 \mu\text{Jy}$. Using a $R = 1.44''$ matching radius, and given the number density of 24 μm sources with $f > 80 \mu\text{Jy}$ in the image, we expect from the P-statistic (Lilly et al. 1999) that approximately one cluster member will be spuriously matched to a 24 μm detection with $f > 80 \mu\text{Jy}$. For non-detections in the

regions of deep and shallower coverage we quote upper limits of $f < 80 \mu\text{Jy}$ and $< 120 \mu\text{Jy}$, respectively. For non-detections located close to bright sources, we assign a larger upper limit of $f < 200 \mu\text{Jy}$.

4. Measurements of star formation histories from optical and mid-IR data

4.1. Optical diagnostics

In this study we focus on the emission feature [O II] $\lambda\lambda 3727$ oxygen doublet and the Balmer absorption line $\text{H}\delta$ as indicators of the star formation rate (SFR). As discussed in P99 and D04, these two features measure the time-averaged SFR over $\tau \sim 10^7$ yr and $\tau \sim 10^9$ yr, respectively. Measurements of [O II] and $\text{H}\delta$ from our sample spectra have been done with a semi-automated line-fitting technique, described in Oem08. A quantitative comparison of the strength of these indicators measures whether the star formation rate has been steady over the previous $\tau \sim 10^9$ yr or whether there has been a starburst with a rapid decline in the SFR rate over that timescale. An ongoing starburst is inferred by comparing the current ($\tau \sim 10^7$ yr) SFR to the total stellar mass of the galaxy, through spectral synthesis modeling.

In the following we use the strengths of [O II] and $\text{H}\delta$ to divide galaxies into spectral types which correspond to different histories of star formation (see Oem08, Table 5 for the definition of the types); e(c)’s are galaxies with continuing star formation, k+a’s and a+k’s are moderate and strong post–starbursts, e(b)’s are starbursts with strong optical emission, e(a)’s are dusty starbursts with weak optical emission, k’s are passive, early–type galaxies, and e(n)’s are AGN’s. By starbursts, we shall mean any galaxy whose observed star formation rate is at least a factor of two higher than its long-term average. We shall use the term “post–starburst” to signify any galaxy which had a starburst in the recent ($\tau \lesssim 10^9$ yrs) past, but at the epoch of observation shows no detectable star formation, and buried starburst to signify a starburst which is sufficiently obscured by dust to completely hide its [O II] emission.

Oem08 have measured the equivalent width of [O II] in the A851 sample. We convert these equivalent widths to [O II] luminosities by the following steps. (1) Because our optical spectra cover only a fraction of each galaxy, while the Spitzer photometry covers the entire object, we must make some assumption about the distribution of [O II] flux over the face of the galaxy. In the absence of any other information, we assume that the [O II] flux has the same distribution as the visible light. (2) Using the total r magnitudes of the galaxies, we calculate the total F_ν at 6500\AA . (3) Using the shape of our fluxed spectra, we then determine the total F_ν at 3727\AA , and from this and the measured $\text{EW}([\text{O II}])$, we calculate the total flux

in the [O II] line. (4) We then use a standard Λ cosmology to calculate total [O II] luminosity. This method is dependant on our assumption about the spatial distribution of [O II], but the spectra, which come from slits that typically cover $\sim 8 \times 12$ kpc at $z = 0.41$, sample a reasonable fraction of each galaxy in our sample, so the sensitivity of our result to this assumption is probably not severe.

The UV flux from young, massive stars in H II regions ionizes oxygen atoms which then produce [O II] through recombination. Only the hottest stars have sufficient UV flux to contribute, so [O II] flux in an H II region is due mainly to the population of O and B stars. Rates of star formation come from folding in the well-known lifetimes of these stars. Deriving the SFR for stars of all masses requires the adoption of a universal initial mass function — an often-questioned, but yet to be invalidated, assumption. We have employed Kennicutt’s (1998) prescription:

$$\text{SFR } M_{\odot}\text{yr}^{-1} = 1.4 \times 10^{-41} L([\text{O II}]) \text{ ergs s}^{-1} \quad (1)$$

We note that, because this is an average rate that includes lower-luminosity spiral and irregular galaxies less luminous irregular galaxies, we are perhaps overestimating the SFR for our sample — by $\lesssim 40\%$ — which makes this a conservative choice for the purposes of this study. On the other hand, there might be even greater uncertainty just from using this $z \sim 0$ relation on earlier-epoch starforming galaxies. We show below that, despite these uncertainties, we derive approximately equal SFRs from both the Kennicutt [O II] relation and from $24 \mu\text{m}$ for “normal” starforming galaxies (in both A851 and a present-epoch field sample covering the same luminosity range), which is reassuring.

The Kennicutt formulation is sometimes corrected for dust extinction and sometimes not. The relation adopted here is corrected for average dust extinction from [O II] to $\text{H}\alpha$, but not for extinction at $\text{H}\alpha$. Our goal is to compare the SFRs derived from [O II] to the SFR derived from the dust-insensitive $24 \mu\text{m}$ luminosity, so measuring [O II] flux and applying the standard correction to $\text{H}\alpha$ for present-epoch galaxies will show whether the distant starforming galaxies in A851 have an unusual amount of dust and thus more star formation than is evident with optical diagnostics. Because our analysis depends on the relative values of these two indicators, our conclusions are not dependent on a rigorous analysis of the absolute value of extinction in our sample galaxies, which is beyond the scope of this paper.

Measurements of $\text{H}\delta$ strength are comparatively insensitive to dust absorption, because, over the 10^9 yr timescale for which it measures the SFR, the A-F stars that contribute most to the $\text{H}\delta$ signal are expected to have diffused out of the dusty regions in which they were born.

4.2. Mid-infrared diagnostic

Empirically, the total infrared (8–1000 μm) luminosity, $L(\text{TIR})$, correlates reasonably well with other star formation rate tracers in nearby dusty star-forming galaxies (Hunter et al. 1986, Lonsdale, Persson, & Helou 1987, Kennicutt 1986). Far-IR emission arises from grey-body emission of dust heated by hot stars. Since the escape fraction for ionizing photons is low, and the dust cross-section peaks in the UV, the far-IR is essentially a calorimeter of hot young stars (Kennicutt 1986, and references therein). Only at low redshift is it currently possibly to sample fully the long-wavelength SED of galaxies to measure $L(\text{TIR})$ directly. Fortunately, monochromatic luminosities in the rest-frame mid-IR (5–30 μm) range correlate well with $L(\text{TIR})$ at low redshift (Chary & Elbaz 2001, Calzetti 2007), and this correlation has been demonstrated to extend to $z = 1.3$ (Marcillac et al. 2006).

Mid-IR emission is a combination of continuum from small grains plus aromatic features. The luminosity surface density in both the continuum-dominated $\lambda_r = 24 \mu\text{m}$ spectral region and the aromatic-dominated $\lambda_r = 8 \mu\text{m}$ spectral region correlate well with that of extinction-corrected Paschen α (Calzetti 2007); in both cases the 1σ scatter is about 0.3 dex. Figure 3 of Alonso-Herrero et al. (2006) shows a tighter correlation between rest-frame 12 μm and extinction-corrected $P\alpha$, $\sigma \sim 0.1\text{--}0.2$ dex.

At $z = 0.4$, the 24 μm band of MIPS on Spitzer detects rest-frame 15–19 μm . These wavelengths are also dominated by continuum emission from small grains, with a contribution from the relatively weak 17 μm aromatic feature. The rest-frame 15–19 μm bandpass has not been similarly calibrated at $z = 0$ because IRAS had no such band, however, since the 15–19 μm continuum arises from the same small grains that produce the 12 μm and the 24 μm rest-frame continua, the scatter in this band should be similar. We conclude from the results from Calzetti, Marcillac et al., and Alonso-Herrero et al., and also Smith et al. (2006, 2007) that the continuum emission in this region should trace the star formation rate with only moderate dispersion. Because mid-IR photons are not further absorbed by other dust grains in starforming regions, they provide a clear view of the total star formation in the system, which [O II] and even $\text{H}\alpha$ cannot do.

In the next section we will use template SEDs generated by Chary & Elbaz (2001) and Dale & Helou (2002) that model the flux distribution from the mid-to-far IR to derive the total SFRs for our detected galaxies. The SED shapes of these templates vary smoothly as a function of mid-IR luminosity, allowing a reliable correction to bolometric IR emission from observations over a relatively narrow wavelength range. A small complication is that these templates do not include $\lambda > 15 \mu\text{m}$ aromatic features. This means that the 17 μm aromatic feature, which falls in the 24 μm band at the $z = 0.407$ redshift of A851, will not be correctly accounted for. However, the feature has a typical equivalent width of only 0.36 μm (Brandl

et al. 2006), and affects the detected MIPS 24 μm flux density only at the 10% level. This small systematic effect is not important for our results.

For a sample of 59 SINGS galaxies, Smith et al. (2007) observed an intrinsic dispersion in aromatic feature strength compared to the dust continuum. Figure 19 of Smith et al. quantifies how this spectral variation affects 24 μm flux density: at $z = 0.4$ the 10%–90% variation in the spectra of their luminous ($L(\text{TIR}) > 2.6 \times 10^{10} L_{\odot}$) sample causes a $\pm 20\%$ change in the MIPS 24 μm flux density. Thus, flux differences of this magnitude should not necessarily be interpreted as differences in star formation rate, since they may be due to intrinsic spectral variation.

Despite these caveats, the robustness from dust obscuration, the well-behaved nature of the mid-IR continuum (Calzetti 2007), and the relative weakness of the 17 μm aromatic feature makes it a relatively reliable diagnostic of star formation rate in bursting galaxies.

4.3. Deriving star formation rates from mid-IR fluxes.

We converted from observed 24 μm flux density to inferred star formation rate as follows: Chary & Elbaz have derived template SEDs that model the full emission from 8–1000 μm for galaxies with a wide range of mid-IR luminosity. We transformed each of the Chary & Elbaz synthetic templates to the cluster redshift and converted L_{λ} to f_{λ} , assuming a flat cosmology with $h_0 = 0.72$ and $\Omega_{\lambda} = 0.73$. We then computed the 24 μm flux density that would be measured for this template using the MIPS response curve.²

We integrated each template from rest-frame 8–1000 μm to find the total infrared luminosity, and converted that to a star formation rate using equation 4 of Kennicutt (1998). The result is a look-up table, at the cluster redshift, of star formation rate as a function of 24 μm flux density. For the range of detected MIPS flux densities, the corresponding Chary–Elbaz templates were numbers 36 to 75.

This extrapolation from rest-frame 15–19 μm to total 8–1000 μm luminosity necessarily depends on the templates assumed. Since we observe large populations of A stars extending well beyond the starforming regions in galaxies which, we will show, have had significant, long duration starbursts, we considered the extra heating that these might provide. Our modeling included comparing the contribution to mid-IR luminosity from young populations ($\tau \lesssim 10^7$ yr) to intermediate-age populations ($\tau \sim 10^8$ yr). From this we concluded that, for a Salpeter IMF and a single-age Starburst 99 model (Leitherer et al. 1999), the power available in A

²http://ssc.spitzer.caltech.edu/mips/spectral_response.html

stars to heat dust is only $\sim 1\%$ of the power available from O and B stars. Thus, we expect our $24\ \mu\text{m}$ detections to be dominated by O and B stars, even in galaxies with large A star populations.

5. Results

5.1. Detection with Spitzer-MIPS is a strong function of spectral type

In Figure 1 we show the result of our attempt to measure Spitzer $24\ \mu\text{m}$ flux densities for our A851 cluster sample. We plot Spitzer $24\ \mu\text{m}$ flux density versus R-band optical flux for the 96 confirmed members of A851 (see Oemler et al. 2008) that are within the Spitzer field. Figure 1 shows that — even for cluster members, which comprise an essentially volume-limited sample — galaxies are detected over a wide range of luminosity. In other words, we are not picking off only the most luminous objects. Most of the cluster members are not detected; however, this sample includes many galaxies that are not starforming (passive), for which detection by Spitzer at $24\ \mu\text{m}$ is not expected, unless the galaxy harbors an AGN.

The non-detection of galaxies without star formation is seen more easily in Figure 2, from the data in Table 1 which break down the detections by optical-spectral classification. Of the 41 galaxies ‘k’ types that are passively evolving, only 2 are detected. There is nothing in the optical spectra of these galaxies that suggests any activity. It is possible that these could be examples of extremely-dust-hidden star formation, as we find below for some of the putative post-starburst galaxies, or AGN, or both.

5.2. Continuously starforming (“normal”) galaxies are generally not detected

Our A851 cluster sample includes both continuously starforming (CSF), e(c) galaxies as well as starburst (SB) and post-starburst galaxies (PSB). The strength of Balmer absorption lines in an integrated spectrum of a galaxy is key to distinguishing the CSF galaxies from the SB and PSB galaxies. The Balmer absorption line strength is a combination of effects, including: (1) the dominance of Balmer absorption lines in the spectra of A stars, which contribute most of the light in populations of age $\tau \lesssim 10^9$ years; (2) the in-filling of Balmer absorption by Balmer emission from the ionized gas in H II regions excited by OB stars; (3) the migration of A stars from the dust-obscured H II regions of their birth, and the distribution and amount of that dust; (4) the strength and duration of the starburst; and (5) the relative contribution of light from KIII stars — populations older than 2×10^9 years. It is the combination of these effects that results in substantially different spectra for CSF as

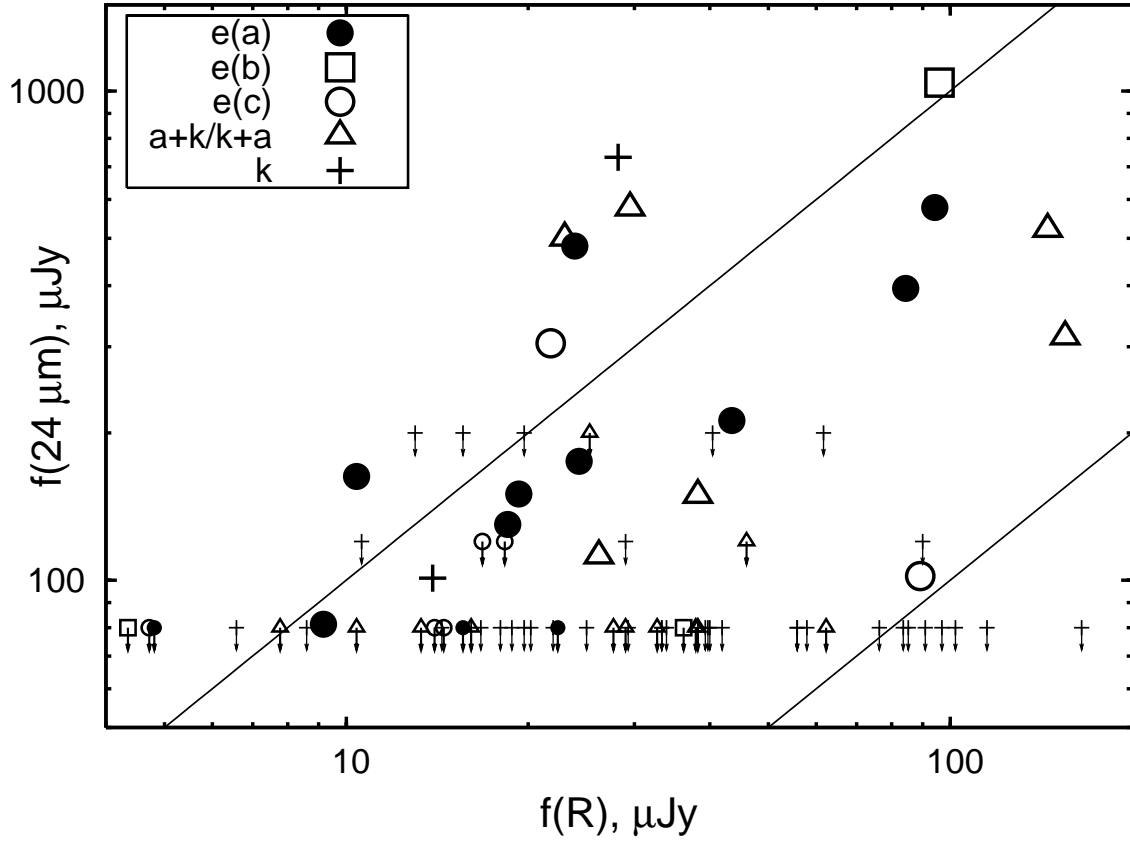


Fig. 1. Spitzer $24\ \mu\text{m}$ flux density vs, optical R-band flux for the cluster members of the optical-spectroscopic sample of A851 galaxies. Most galaxies are undetected by Spitzer: only 2/7 e(c)'s, and 2/41 k's are detected. (The k-types upper-limits are the smaller arrows.) However, 9/12 e(a)'s, 1/3 e(b)'s, and even 6/18 “post-starburst” galaxies, k+a & a+k, are detected, indicating a clear connection between starburst activity and heavily dust-obscured star formation. This figure shows the spread of flux for the sample: a factor of 20 for both the $24\ \mu\text{m}$ observations and the R-band (3.2 mag).

compared to SB or PSB galaxies, the key to distinguishing CSF galaxies from other types.

The part of the A851 cluster sample that is coincident with Spitzer MIPS observations contains 7 CSF e(c) galaxies. Only 2 of these are detected with MIPS. The 7 e(c) galaxies cover the full range of optical and 24 μm luminosity, so this poor detection rate is not mainly due to some luminosity-dependent selection effect. As we show in Section 6, we expect $\text{SFR}(\text{IR}) \sim \text{SFR}([\text{O II}])$ for these galaxies (from a comparable low-redshift, local sample), which would give them 24 μm luminosities scattered around the Spitzer–MIPS detection limit.

5.3. One-third of post-starburst galaxies are detected

The post-starburst galaxies of types “k+a” and “a+k” are also mostly undetected, but the fraction 6/18 that are detected is significantly higher than even that of the e(c) galaxies, so this is a surprisingly high rate for galaxies that are supposed to be observed *after* star formation has completed. The fact that some of these post-starburst galaxies could have substantial star formation hidden by dust, particularly in their nuclei, had been previously suggested by detections in the radio continuum (Smail et al. 1999), preferentially of objects with the strongest $\text{H}\delta$. These a+k galaxies also show the broadest $\text{H}\delta$ absorption lines, indicative of the youngest A-star populations (closest in time to the burst) — see D04 and Oem08. Of the a+k galaxies in the Spitzer field, 2/5 are detected, compared to only 4/13 of the k+a, but with such a small sample, this is only suggestive.

The Spitzer data, then, lead to two important results for the post-starbursts: (1) Most of the galaxies classified as post-starburst are exactly that — there is little or no ongoing, hidden star formation ($\text{SFR} < 3 M_{\odot} \text{ yr}^{-1}$). This removes a critical uncertainty in earlier work. (2) A significant minority of cluster galaxies classified as post-starburst hide some residual star formation. A few of these may be as active as the starbursts we discuss next, but as we show in Section 7 (where we model the history of star formation), for most the rate of residual star formation is much lower than the preceding burst. It is quite possible that this remaining dust-obscured star formation is concentrated to the center of the galaxy — this is perhaps the only location where a very high extinction can be supported — while the previous, larger starburst might have been a more global, and thus more powerful event.

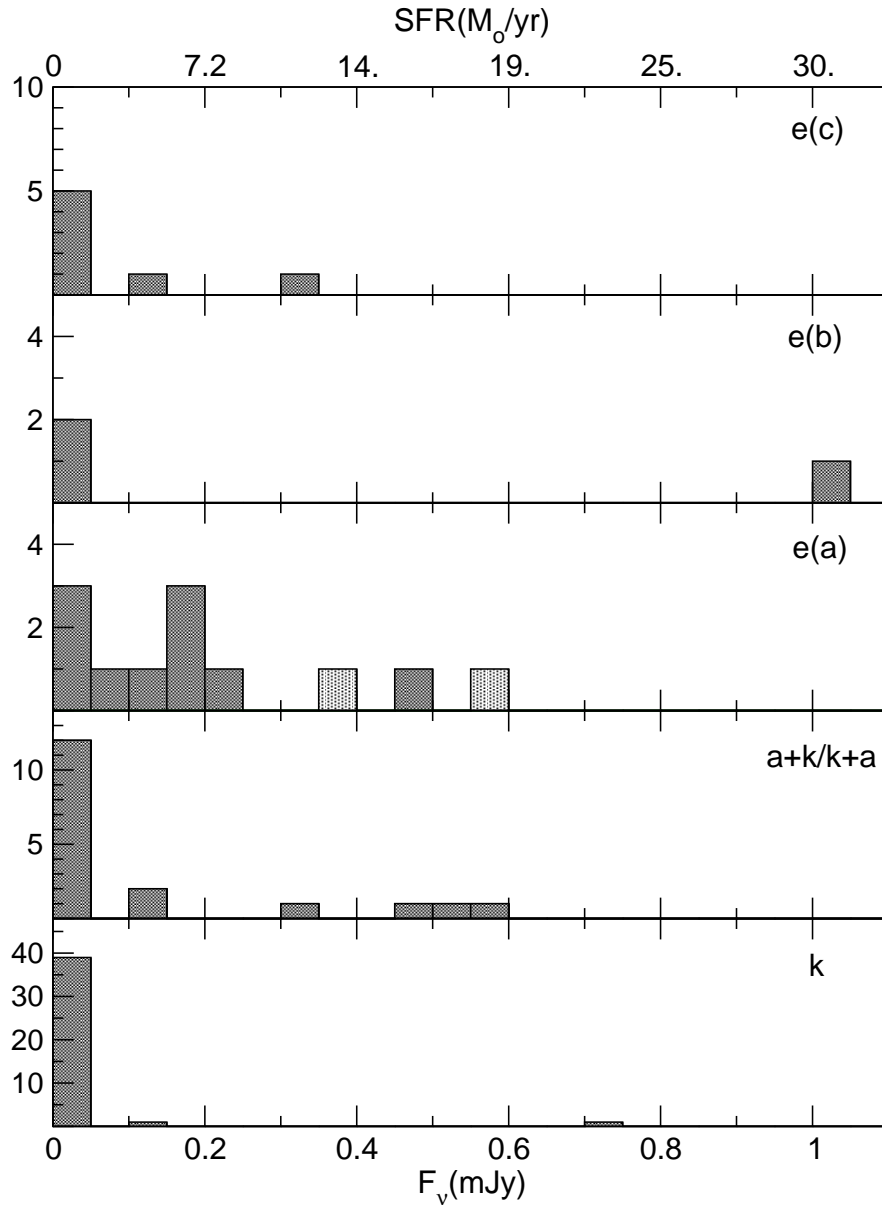


Fig. 2. The distributions of “detectability” as a function of the spectral type. The horizontal axis is labeled in $24\ \mu\text{m}$ flux density (below) and star formation rate (above). The only type for which a majority of galaxies (9/12) is detected is the e(a) class — the putative dusty starbursts. (The two lightly shaded squares are k+a galaxies with $[\text{O II}] \approx -4\ \text{\AA}$, slightly below the threshold for the class defined in P99.) The least detected are k-types (2/41) — passively evolving early-type galaxies. Most post-starburst galaxies are not detected, as expected, but 6/18 are, suggesting that some members of this class are still actively forming stars well hidden by dust. Only 2/7 of the e(c) galaxies; some may lie just below the detection limit (but this could also be the case for the 3 undetected e(a) types). Of the 3 e(b) galaxies in this sample, only 1 is detected. Forgetting the small-number statistics, this might seem surprising, however, the one detected e(b) is a high-luminosity system, while the others are much less luminous, and likely less dusty (as evidenced by the strong emission lines).

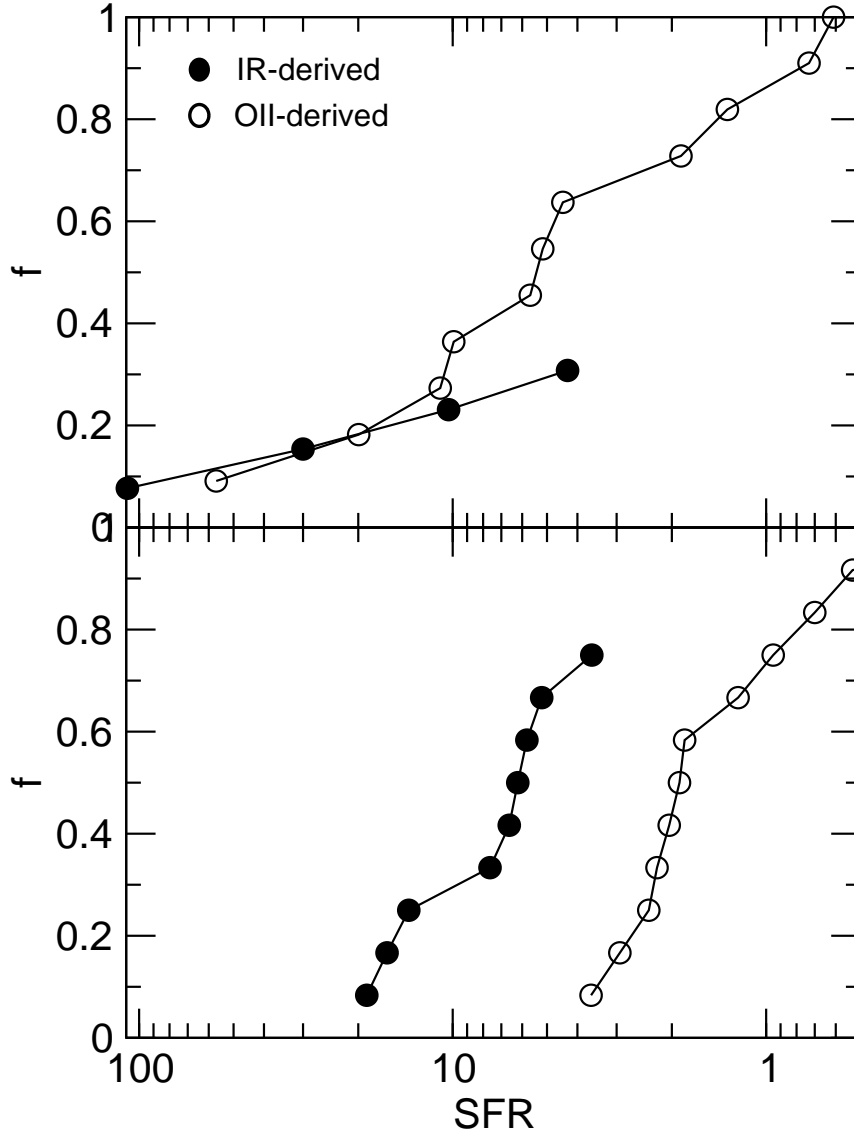


Fig. 3. The cumulative distributions of star formation rates (SFRs) for the galaxies in A851 measured from Spitzer $24\ \mu\text{m}$ fluxes and [O II] emission lines. The data are for all galaxies with $\text{EQW}(\text{OII}) < -4$ angstroms. Galaxies in which $\text{EQW}(\text{H}\delta) < +4\ \text{\AA}$ — e(c) — are shown in the upper plot; galaxies with $\text{H}\delta > +4\ \text{\AA}$ — e(a) — are shown on the bottom. The weak Balmer absorption of the upper sample is indicative of normal, continuously starforming galaxies, while the bottom is a sign of starburst activity. The line with open circles shows the cumulative distributions of SFRs derived from [O II], and the line with solid points shows the distribution with SFRs derived from $24\ \mu\text{m}$. The lines trace each other in the upper plot — both methods measure the same SFR, but in the starbursts of the lower plot show an offset that corresponds to a factor of 4 greater $\text{SFR}(24\ \mu\text{m})$ compared to the $\text{SFR}([\text{O II}])$. In other words, starburst galaxies — as identified by $\text{H}\delta$ absorption — have a majority of their star formation obscured by dust, while continuously starforming galaxies do not.

5.4. Candidate “active starburst” galaxies – the majority are detected!

As explained in Section 2, our hypothesis has been that e(a) galaxies, which show both strong H δ and some [O II], are active starbursts that feed the post-starburst population. Because the [O II] strength of these systems is insufficient to indicate a starburst, this only makes sense if most of their star formation is hidden by dust. The Spitzer 24 μm data for A851 confirm that hypothesis — for this cluster, at least. For the e(a) galaxies, 9/12 are detected.³ This is our major result.

To quantify what this means for the amount of star formation that has been dust-obscured, we calculate independently SFRs from [O II] and from 24 μm , as described in Sections 4.1 and 4.2. Because there is considerable uncertainty in the measurements for each individual galaxy (the calibrations will depend on average values of dust temperature and UV-excitation by young stars, for example), we show in Figure 3 the result of this comparison as a cumulative distribution of SFRs for both indicators. We plot only the galaxies for which [O II] is detected, [O II] $\leq -4 \text{ \AA}$. The upper panel is for weak H δ absorption, what we identify as CSF — spectral type e(c) — starting at $1 M_{\odot} \text{ yr}^{-1}$ in the upper right corner and proceeding to very high rates of star formation for a few galaxies in the 10’s of $M_{\odot} \text{ yr}^{-1}$. The solid points show the rates inferred from the [O II] indicator, the open circles, the 24 μm indicator. The fact that the two lines closely follow each other means that approximately the same star formation rate is measured with both indicators: $\text{SFR}(24 \mu\text{m})/\text{SFR}([\text{O II}]) \sim 1$.⁴

The situation for the H δ -strong, starbursting galaxies is very different. The two lines track each other, but with a clear offset: $\text{SFR}(24 \mu\text{m})/\text{SFR}([\text{O II}]) \sim 4$. In other words, the 24 μm flux indicates an SFR that is, on-average, a factor of 4 greater than is indicated by the [O II] emission line, a sufficiently greater SFR that these qualify as the active, moderate starbursts that feed the post-starburst galaxy population. In the next section we show that $\text{SFR}(24 \mu\text{m})/\text{SFR}([\text{O II}]) \sim 1$ is typical of local, present-epoch, continuously starforming galaxies, whereas those with $\text{SFR}(24 \mu\text{m})/\text{SFR}([\text{O II}]) \sim 4$ — the low end of today’s LIRGs

³This includes 2 galaxies that we detected in [O II] with an equivalent width of [O II] $\sim 4 \text{ \AA}$. This would have placed them in the k+a category previously, but in the context of studying SFR from [O II], it makes more sense to include them as e(a) galaxies here, because their weak [O II] flux is the result of extinction, not a low star formation rate.

⁴Because of the inclusion of a partial extinction correction in the Kennicutt relation for $\text{SFR}([\text{O II}])$, $\text{SFR}(24 \mu\text{m})/\text{SFR}([\text{O II}]) \sim 1$ occurs at an extinction of about 0.9 mag at [O II], calculated for a foreground screen (see Kennicutt 1998). Equality of these two derived star formation rates does not mean that star formation is completely unobscured, but is attenuated by dust as is typical for a present-epoch spiral galaxy.

— are relatively rare.

6. Comparison with local samples of starforming galaxies

Based on the [O II] and H δ spectral indices, P99 and D04 have argued that moderate starbursts — like those in A851 we are discussing here — are a common feature of the intermediate-redshift galaxy population, both cluster and field. The Spitzer–MIPS data for A851 give us an opportunity to investigate this claim and remove the uncertainty of dust-obscured star formation to which the optical indicators are more prone. In order to demonstrate that the prevalence of dust-obscured starbursts at $z \sim 0.4$ is an epoch-dependent effect, we need to compare to a like sample of starforming galaxies at the present epoch. Do present-epoch starforming galaxies mostly have $\text{SFR}([\text{O II}]) \sim \text{SFR}(\text{IR})$, indicating that the modest extinction assumed in deriving $\text{SFR}([\text{O II}])$ applies? Or, do many of them have a majority of their star formation hidden by dust, so that $\text{SFR}(24 \mu\text{m}) \gg \text{SFR}([\text{O II}])$?

Despite the proliferation of local galaxy surveys, constructing a local comparison sample is not easy. To begin with, we cannot use present-epoch rich clusters as a source, since these contain very few starforming galaxies of mass $M > 10^{10} M_{\odot}$; this is the Butcher-Oemler effect, the point at which we started. We must instead use galaxies in the field — isolated and in groups — to judge if the characteristic *mode* of star formation, as well as its amount, has changed over time.

Another difficulty is that we need both 24 μm observations and [O II] fluxes that cover the full disk of each galaxy in order to correspond to the distant cluster data. The survey that comes closest to this is a study of 417 starforming galaxies by Moustakas & Kennicutt (2006). In this study, [O II] fluxes were obtained from observations for which the slit of the spectrograph was scanned across the galaxy in order to obtain an integrated [O II] flux, as we obtain by necessity for intermediate-redshift galaxies by using ~ 1 arcsec-wide slits. Unfortunately, this survey is not volume limited, but rather it was chosen to represent many different galaxy types: not only normal galaxies, but also starbursts, peculiar galaxies, interacting/merging systems, and dusty, infrared luminous galaxies were handpicked for inclusion. As a result, we were not able to use this study to assemble a sample, based on optical luminosity alone, that was complete in any volume-limited sense.

However, the Kennicutt-Moustakas survey provides data that does allow us to construct such a sample. In Figure 4 we show total U-band flux vs integrated [O II] flux for all galaxies from that survey for which both measurements are available. Fluxes are from the tables of Moustakas & Kennicutt (2006), which for U-band is generally taken from

RC3 (deVaucouleurs et al. 1995), and correspond to total magnitudes, that is, photometry through fixed apertures has been used to extrapolate a total brightness for the galaxy in the U-band. The strong correlation is due to the fact that the UV flux arises from the hot young stars that power [O II] emission from the H II regions. Even with the ambiguity of dust absorption/obscuration, the fact that these two indicators arise from the same spatial regions assures a good correlation. From the data in Figure 4, we fit a relation between integrated U-band photometry and integrated [O II] emission, so that we can use U as a proxy for OII:

$$\log L([\text{O II}]) = M(\text{U-band})/-2.5 + 32.8404 \quad (2)$$

Next, we construct a volume-limited local sample of galaxies using the NASA/IPAC Extragalactic Database (NED), as follows. We use an “Advanced All-Sky” NED query, restricting the velocity to $1000 \text{ km s}^{-1} < v < 2500 \text{ km s}^{-1}$, and select the 241 galaxies with absolute magnitude $M_V < -19.5$. We remove galaxies whose morphological type is listed as E or S0.⁵ For the remaining 133 galaxies, we took photometric measurements from NED: 112 had a total U-band measurement (all but 5 from the RC3), and 94 were detected by IRAS at $25 \mu\text{m}$. (The several-arcminute beamsize of IRAS means that the mid-IR flux is also an integrated quantity.) We convert U and $25\mu\text{m}$ fluxes to absolute U-band magnitude and monochromatic $25\mu\text{m}$ luminosity using the velocities listed in NED, assuming pure Hubble flow and $H_o = 72$. Since the IRAS survey was all-sky, and 85% of the sample has tabulated U-band data, this sample is for the present purpose volume limited and unbiased.

U-band absolute magnitudes were converted to [O II] luminosities using eqn. 2, and from that to SFR using the Kennicutt (1998) relation. IRAS $25\mu\text{m}$ luminosities were converted to $L(8-1000\mu\text{m})$ using the relation we fit to the Chary & Elbaz (2001) models:

$$\log L(8-1000\mu\text{m}) (L_{\text{sun}}) = 0.89942 * (\log L_{\nu}^{25} (L_{\text{sun}}) + 1.77782) \quad (3)$$

and from there to SFR using the relation from Kennicutt (1998).

To make the most straightforward comparison to the A851 sample, in Figure 5 we plot $\log \text{SFR}(\text{IR}) - \log \text{SFR}(\text{U})$ versus M_V for the local sample. For local galaxies corresponding to the absolute magnitude distribution of our A851 sample, $-22 < M_V < -19.5$, we find that, on average, the $\text{SFR}(\text{IR}) \lesssim \text{SFR}(\text{U})$. That is, we find few galaxies comparable to the $\text{SFR}(\text{IR})/\text{SFR}([\text{O II}]) \sim 4$ that we found to be typical of the e(a) galaxies in A851, those identified as starbursts. Rather, we find the local sample to cluster around $\text{SFR}(\text{IR})/\text{SFR}(\text{U}) \sim 1$, values that we found for the e(c) galaxies in A851 — galaxies without starbursts. There appears to be a rising trend in $\text{SFR}(\text{IR})/\text{SFR}(\text{U})$ for the faintest objects in the local sample,

⁵This large percentage reflects the prominence of the Virgo Cluster.

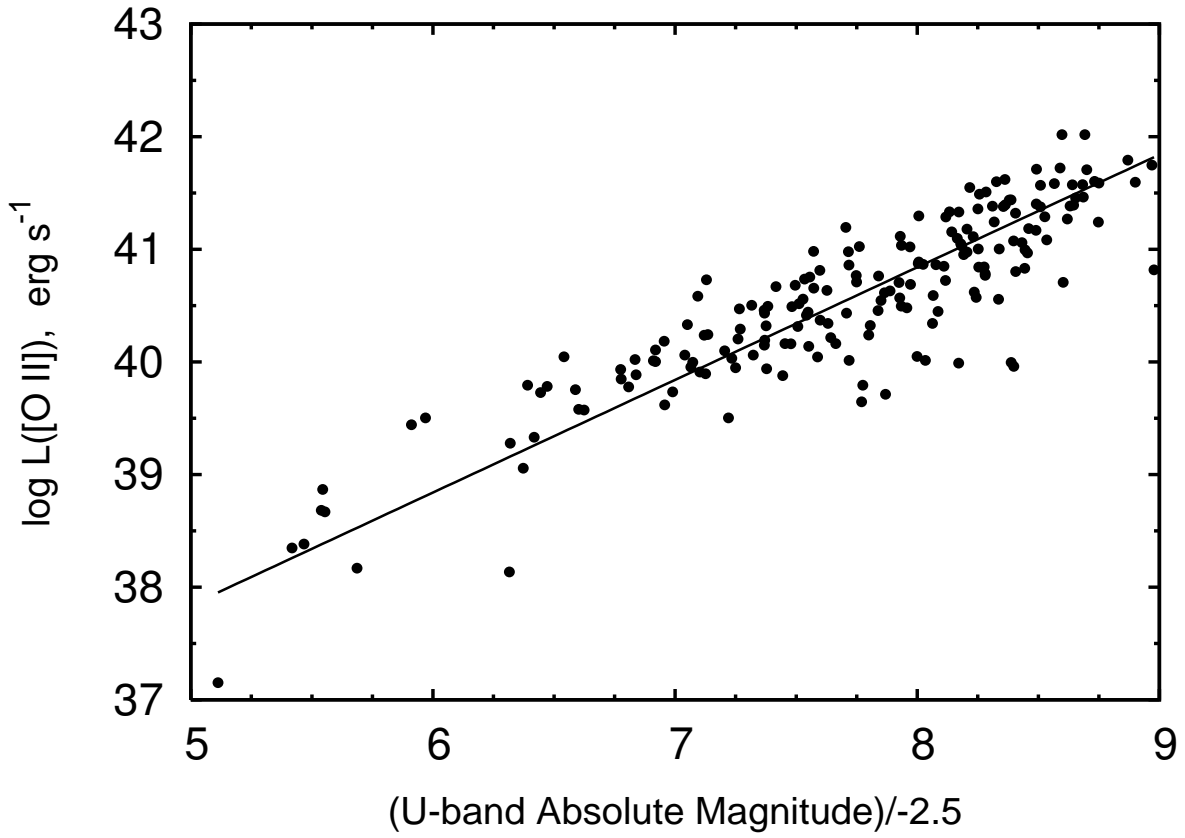


Fig. 4. U-band flux versus [O II] flux for the Moustakas & Kennicutt (2006) sample of local starforming galaxies. The [O II] spectra are unique in that the spectrograph was scanned over a large fraction of the galaxy. The solid line is the best-fit line of unity slope, with coefficients given in eqn. 2; this relation lets U-band flux be used as a proxy for [O II].

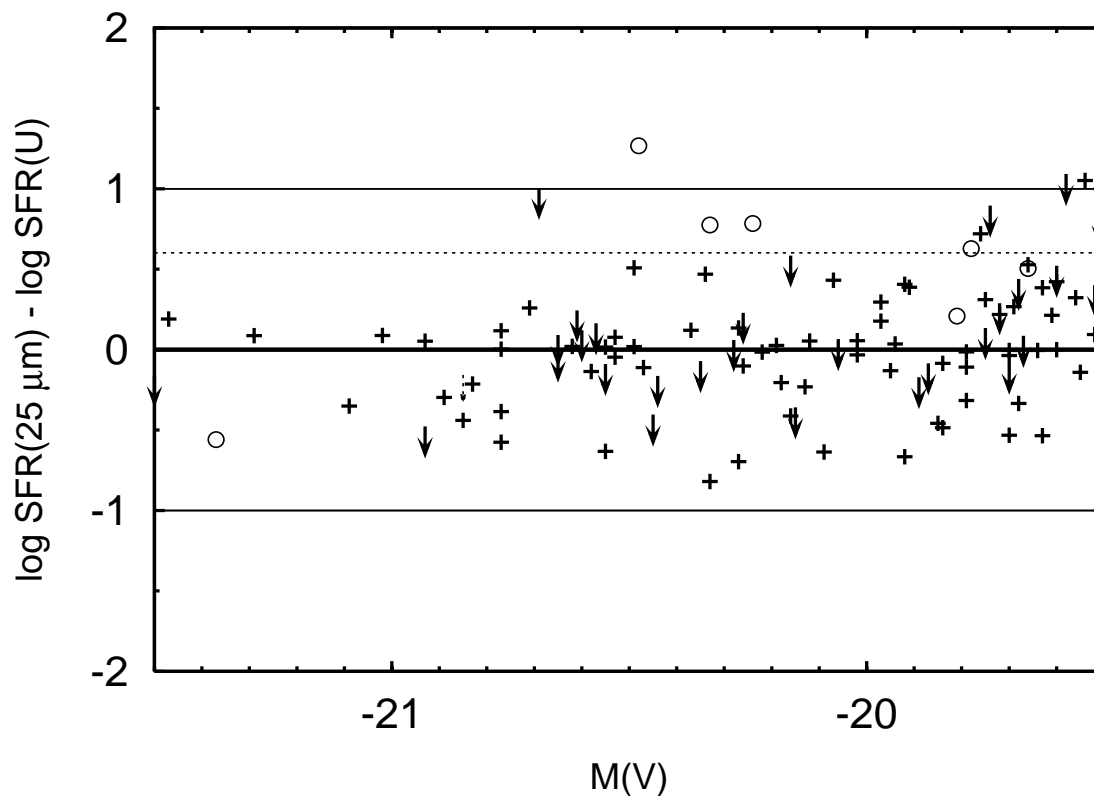


Fig. 5. Comparison of U-band and $25\mu\text{m}$ -derived star formation rates for the local volume-limited sample, using the [O II] vs. U-band calibration (Fig. 4). The typical luminous ($M_V < -19.5$) starforming galaxy in the local sample has $\text{SFR}(\text{IR})/\text{SFR}(U) \sim 1$, in other words, the optical measurement of the star formation rate is consistent with the SFR determined from the mid-IR. This suggests that dust obscuration is moderate for a typical present-epoch spiral or irregular galaxies. Only a few galaxies show significantly enhanced $\text{SFR}(\text{IR})/\text{SFR}(U) \sim 3$, indicative of a high level of dust obscuration, whereas the *average* $\text{SFR}(\text{IR})/\text{SFR}(\text{OII}) \sim 4$ for the distant galaxy sample with the starburst signature. Open symbols represent known AGNs, which are excluded because their mid-IR fluxes are not mainly a product of star formation. The errors in this plot are dominated by extrapolation to total U-band magnitudes, which are typically 20% or less.

but the IRAS sensitivity limits begin to be important, and these are, at any rate, fainter than the galaxies in our A851 sample.

As we suggested earlier, finding $\text{SFR}(U) \approx \text{SFR}(24 \mu\text{m})$ for the large local sample and the relatively small e(c) sample in A851 supports the claim that we are dealing with the same kinds of objects, and it also indicates that our $24 \mu\text{m}$ SFR diagnostic is reasonably good.

From our small but complete sample, we can see that for typical, present-epoch, star-forming galaxies, star formation is only moderately obscured by dust. While it is not hard to find galaxies that are significantly dust-obscured today, they account for only a few percent of the local population (see, for example, Rieke & Lebofsky 1978). For the Morphs ten-cluster sample, Dressler et al. (1999) found a typical fraction of e(a) galaxies of 10 – 20%. Assuming the association of dusty starbursts with e(a) spectra we find in A851 is representative of this larger sample, this points to a factor of ~ 4 decrease in the number of dusty starbursts in the last 4 Gyr, a relatively short time in cosmic terms.

7. The star formation histories in A851 galaxies

The next step should be to analyze the spectra of our galaxies to see what the heuristic distinctions ‘starburst, post-starburst, and ‘continuously starforming’ really mean in terms of star formation histories. Our data for this study is minimal for this purpose, but here we develop the tools in anticipation of the much larger, higher quality data set to come.

Our A851 galaxies have on-average low S/N spectra, so we follow the technique of Dressler et al. (2004) to increase the S/N substantially and create representative templates of each class. We use the spectrophotometric model of Fritz et al. (2007) to analyze the composite spectra in order to derive approximate star formation histories of the various classes. The model performs a simultaneous fit to the stellar continuum and to a number of emission and absorption features in each observed composite spectrum, as well as to the total IR luminosity, as derived by the $24 \mu\text{m}$ flux (Section 4.3). For the A851 composites we substituted the broad-band fluxes in place of the optical continuum shape, due to uncertainties in the relative flux calibration of these spectra.

The program measures equivalent widths of absorption and emission features in the modeled, synthetic spectra in the same way as is done for the observed spectrum. This requires that, in performing the fit, spectra representing a single stellar population, or SSP, are degraded to the resolution of our observed spectra, and also that spectral regions with sky-subtraction problems are excluded. The result is a sum of single stellar populations

(SSPs) that minimize a χ^2 function that measures the differences between the model and the observed values of the observables. The fitting algorithm is discussed in detail in Fritz et al. .

Dust obscuration is allowed to vary with stellar age, to account for the fact that younger stars are generally more obscured than older ones. Three metallicities — solar, $Z=0.05$, and $Z=0.004$ — are explored when searching for the best fit. For each value of SSP metallicity, we perform 11 different fits of the same observed spectrum changing both the initial point in the parameter space and the seeds of the random number generator, to evaluate the robustness of our results and the “spread” in parameter space (i.e., in star formation history) of all acceptable solutions. We choose the metallicity yielding the best χ^2 . Among the 11 models of that metallicity, we choose as reference model the one that has the median value of the total stellar mass: all the quantities quoted in this paper, such as masses, star formation rates, and extinction values, refer to this model. Error bars are computed as the half-difference between the two models (among the 11) with the most disparate values of total mass from the reference model. Details on the error determination for the SFRs computed by our model can be found in Fritz et al. (2007). The model employed here uses the new MILES observed stellar library from Sanchez-Blazquez et al. (2006) and a Salpeter IMF with stellar masses in the range $0.15 \leq M/M_{\odot} \leq 120$.

Finally, since not all galaxies are detected by Spitzer-MIPS, we explored two cases: one in which the non-detections correspond to an IR luminosity = 0, and one adopting as IR emission the upper limit of our Spitzer data, $SFR = 3 M_{\odot}\text{yr}^{-1}$. These two cases should bracket the possible range of star formation rates acceptable, and allow us to assess the uncertainty in the conclusions due to the unmeasured IR fluxes.

By determining the contribution of SSPs of different ages, the model yields a star formation history. That is, the mass formed at each cosmic time up to the epoch of observation, the extinction by dust and the total stellar mass for each composite spectrum. The synthetic spectra computed by the model are compared to the input composite-spectra observations in Figure 6. In the next sections we discuss each of these classes and the SFR histories that have been derived.

7.1. Post-starburst spectra

Post-starburst spectra with and without a Spitzer-MIPS detection have been modeled separately in order to compare their star formation histories. In the following discussion we will use the term “observation epoch” — OE — to refer to the properties of galaxies as

observed at the lookback time, for this case, approximately 4 Gyr ago.

The Spitzer-detected, post-starburst (k+a) composite spectrum is best fitted by a population of age $\tau > 6 \times 10^9$ years that comprises 70% of the OE galaxy stellar mass, followed by a strong burst occurring over $2 - 5 \times 10^8$ yr before OE that produced most of the remaining 30%. The IR detection by itself indicates residual continuing star formation at the OE (Figure 7). The average galaxy stellar mass for this type was $M = 1.50 \times 10^{11} M_{\odot}$. The average SFR per galaxy was about $16 M_{\odot} \text{ yr}^{-1}$ over the galaxy’s history, but during the last $\tau \lesssim 6 \times 10^8$ yr, the SFR was considerably higher, $72 M_{\odot} \text{ yr}^{-1}$. More recently, over the last 2×10^7 yr before OE, the rate was $9 - 10 M_{\odot} \text{ yr}^{-1}$, significant in absolute terms, but substantially less to the extended high rate of star formation that preceded it. To summarize in words, the IR-detected post-starburst galaxies are galaxies that have experienced a substantial burst of star formation — significantly above the long-term past average — followed by a level of ongoing star formation that is significant in absolute terms, but a sharp decline from the previous burst.⁶

Our model for the *IR-undetected* post-starburst (k+a) spectrum confirms a substantial burst that is followed by a low-to-zero level of residual star formation (depending on how the IR non-detections are handled). The average SFR per galaxy in this group is $\sim 12 M_{\odot} \text{ yr}^{-1}$ over the typical galaxy’s history, rising by a factor of 3.3 (1.4) to 39 (17) $M_{\odot} \text{ yr}^{-1}$ (the first number corresponds to setting IR flux = 0, while the number in parentheses corresponds to setting the IR flux = upper limit) during the last 6×10^8 yr, and 0.0 (0.9) solar masses per year during the last 2×10^7 yr. In words, the burst of star formation represents a significant rise over the past average, and there is no significant star formation at the epoch of observation — a definite post-starburst.

The average galaxy stellar mass for this class is somewhat lower than for the Spitzer-detected post-starbursts, yielding $1.1 \times 10^{11} M_{\odot}$ regardless of the IR limits adopted, while the mass fraction formed during the last 6×10^8 yr varies significantly depending on whether no

⁶Though the equivalent widths of the spectral features and the broad-band continuum fluxes can be reproduced, our model fails to account for the broadness of the Balmer lines in Spitzer-detected a+k/k+a, as can be seen in Figure 6 (second spectrum from the top). We found no single SSP or combination that was able to account for this. We simulated the effects of an high velocity dispersion of 250 km s^{-1} for the galaxy, by convolving our SSPs with a Gaussian. The top spectrum of Figure 6 shows the best fit star formation history and rate unchanged with respect to the unbroadened fit, however, the line width is now reproduced. The broadening of the lines due to high galaxy velocity dispersions is consistent with the high average galaxy stellar mass found by both types of fits, $M = 1.5 \times 10^{11} M_{\odot}$. This mass agrees well with the value expected for early-type galaxies: assuming $M/L = 4$ (at the low end of the range for early type galaxies, and thus appropriate for this post-starburst example), the predicted velocity dispersion from a modern determination of the Faber-Jackson relation in the Coma cluster (Matkovic and Guzman 2007) is $\sigma = 230 \text{ km s}^{-1}$.

IR emission or IR upper limits are included in the fit, $\sim 20\%$ versus 9% .

The post-starburst galaxies with and without a Spitzer detection have in common a history where a significant fraction, $10 - 30\%$ of the galaxy mass has formed in a recent burst with exceptionally high star formation rates. A lower limit for the SFR *during* the burst can be estimated from the average SFR during the last 6×10^8 yr, thus $\text{SFR} > 20 - 70 \text{ M}_\odot \text{ yr}^{-1}$.

7.2. Emission-line spectra

The star formation history that best fits the e(c) “continuously starforming galaxy” composite spectrum is markedly different from the two similar starburst histories described above. The average SFR per galaxy in this group is about $7.5 \text{ M}_\odot \text{ yr}^{-1}$ over the typical galaxy’s history, between 1.6 (0.6) $\text{M}_\odot \text{ yr}^{-1}$ (null IR flux or upper limit) during the last 6×10^8 yr and 2.1 (1.5) $\text{M}_\odot \text{ yr}^{-1}$ during the last 2×10^7 yr before OE. Recent and ongoing SF levels are low, significantly lower than the all-time past average. It is important to stress that the variations of SFR over a single stellar population should not be considered significant, as the model cannot have such detailed time resolution. The overall SFR trends, as quantified in the broad age intervals of which will be presented in Table 2, are significant, but smaller intervals with higher or lower SFRs are not. For example, in the case of the e(c) galaxies, we note that the observed composite spectrum is noisier than in the post- or dusty- starburst composites, due both to the small number of objects (7) and their relative faintness. The full star formation history shown in Figure 7 for the e(c) shows many ups and downs, but these are not statistically significant. The overall star formation history — with these data — can best be interpreted as strong in the first few Gyr ($z \sim 2$) and steadily declining thereafter. Unlike the post-starbursts discussed above, and the dusty-starbursts discussed next, there are no important bursts for many Gyr before OE.

The stellar mass determined by the model for the average galaxy in the e(c) group is around $7 \times 10^{10} \text{ M}_\odot$, lower than the either of the post-starburst types discussed above.

The average galaxy mass is even lower for the fit of the e(a) “dusty-starburst” spectrum: for the typical galaxy in this class $M = 2.5 \times 10^{10} \text{ M}_\odot$. The model history of the dusty starbursts is consistent with an all-time average SFR per galaxy of 2.7 (2.8) (null IR or upper limit), while the recent and ongoing SFRs are 6.4 (6.6) during the last 6×10^8 yr and 6.9 (7.3) during the last 2×10^7 yr. The recent star formation in these galaxies is therefore more than twice the all-time average. The rise in SFR compared to the $\sim 10^9$ years immediately preceding the burst might actually be more than a factor-of-two, because most massive galaxies show histories of monotonically declining SFR over time, in other words, using the

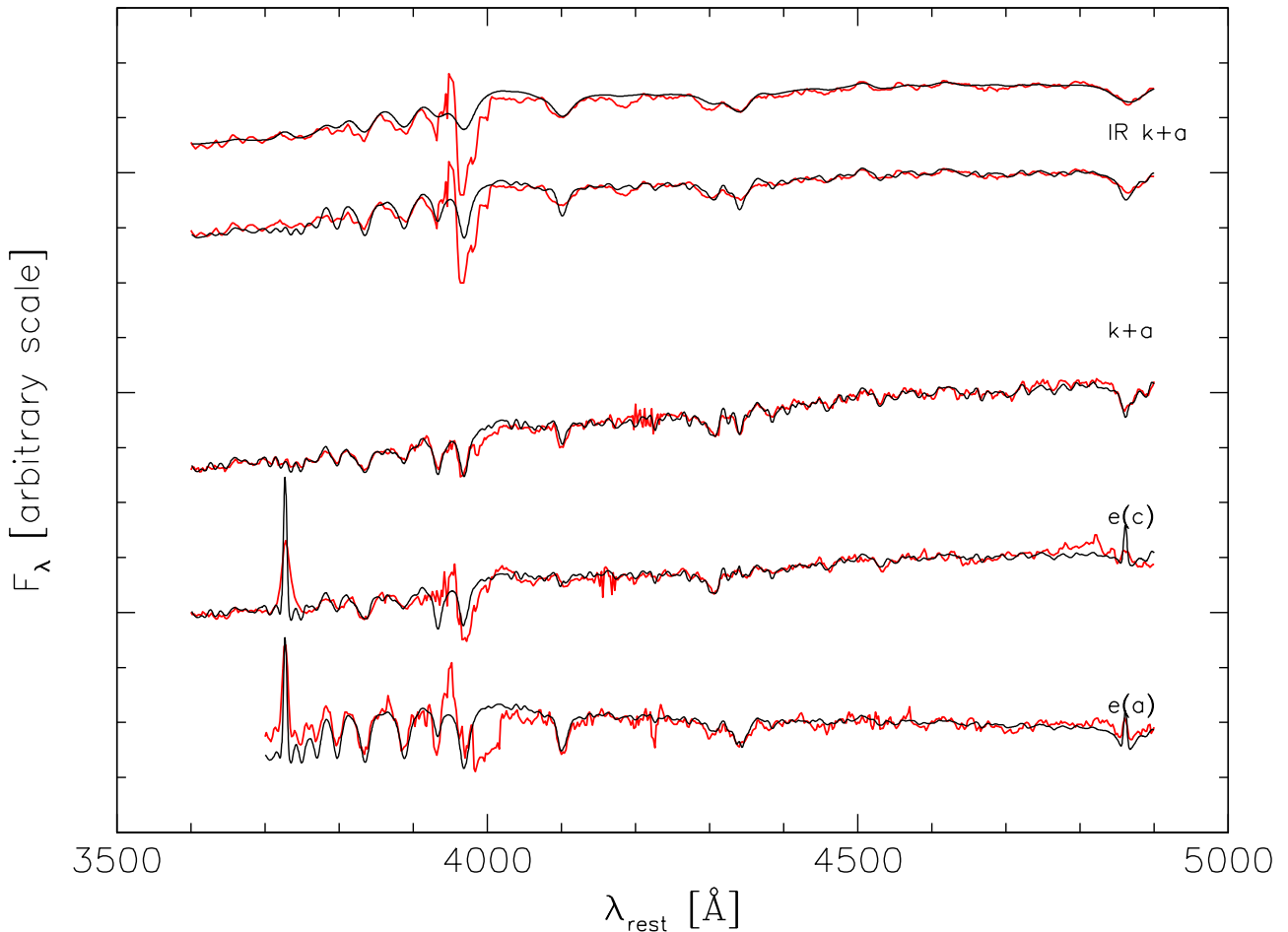


Fig. 6. Observed composite spectra (red, thick line) compared to models (overlaid, thin black line). From top to bottom: post-starburst galaxies with and without IR emission, of starforming galaxies and dusty starbursts. Broad-band galaxy photometry, rather than the spectroscopic continuum, was used in the fitting procedure. The fits were to these broad band colors and the equivalent widths of the emission and absorption lines, not the shape of the lines. The line shape fits are acceptable except for the infrared post-starburst spectrum (IR k+a), which has significantly broader Balmer absorption lines than the model. The bottom of the two templates for IR-detected k+a galaxies shows a poor fit to the width of the Balmer absorption lines. The top spectrum shows that we are able to reproduce the Balmer line profiles by smoothing the model fit to correspond to a velocity dispersion of 250 km s^{-1} , which is appropriate for elliptical galaxies of the mass of the average k+a in the composite.

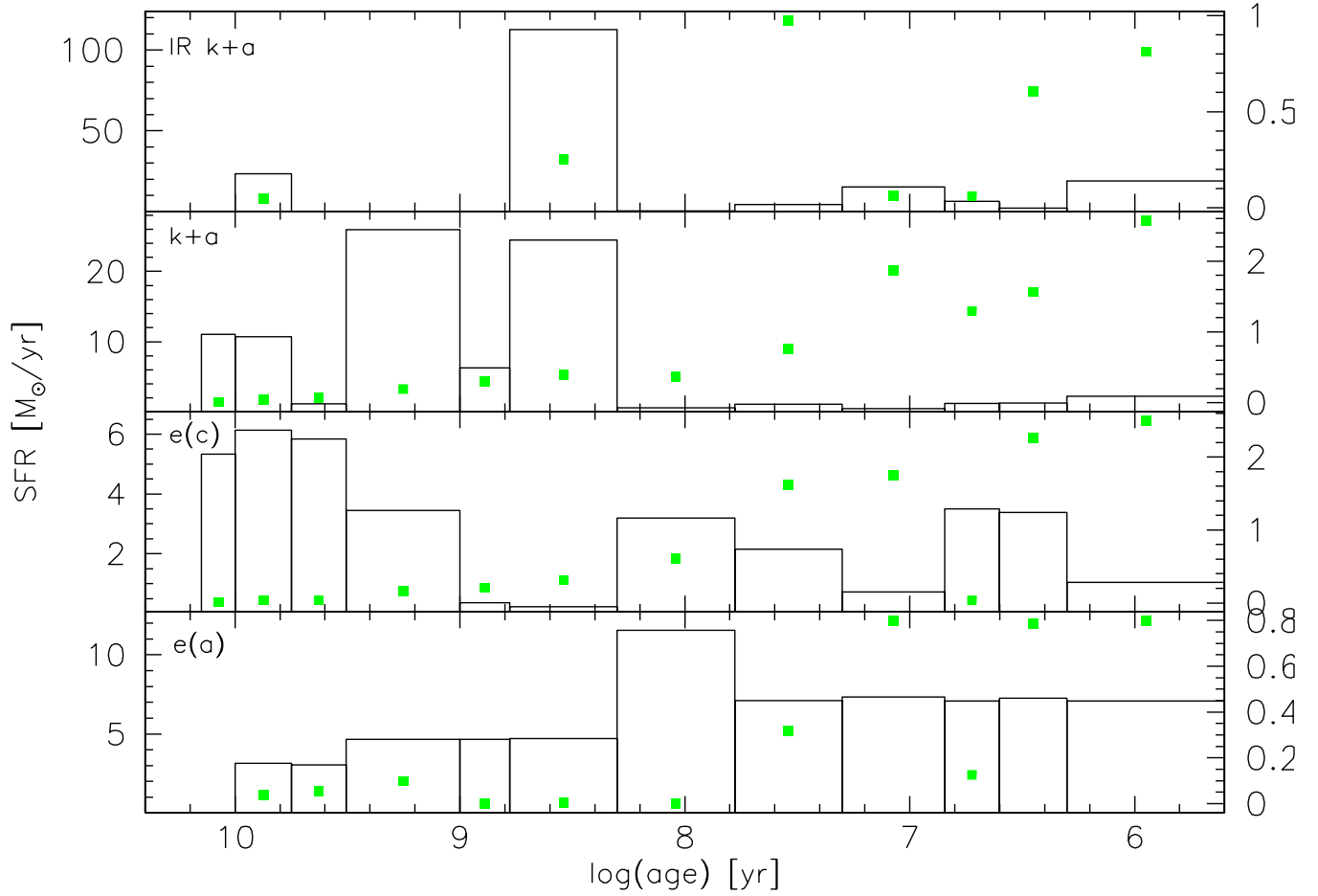


Fig. 7. Star formation rate as a function of SSP age for the best-fit models of post-starburst galaxies with IR emission (IR k+a), post-starburst galaxies without IR emission (k+a), starforming galaxies [e(c)], and dusty starbursts [e(a)]. SFRs are in $M_{\odot}\text{yr}^{-1}$, averaged over the number of galaxies of each spectral class. Age = 0 corresponds to the epoch of observation. Green dots indicate the value of $E(B-V)$ for each stellar population, with the scale shown on the right.

“all-time” average is likely to be an upper limit for the period immediately preceding the burst. The modeling cannot, without very high S/N spectra, resolve this difference, but a more accurate assessment of the rise in SFR compared to the time immediately preceding the burst, would be important in understanding the actual physical conditions and mechanisms that might be responsible.

In summary, the e(a) galaxies have had starbursts like the k+a types, but these starbursts – substantially hidden b dust — are continuing at the OE.

Table 2 contains a summary of the model results for each of the different spectral classes, including the SFR per galaxy averaged over the last 2×10^7 , 6×10^8 and over the age of the universe at $z = 0.4$ (“all-time”), $\tau = 9.2 \times 10^9$ yr). Also listed is the number of galaxy spectra which contributed to each composite spectrum. The classification into spectral classes has clearly identified galaxies with markedly different stellar histories. The k+a galaxies are once more confirmed to be post-starburst galaxies, with or without (depending on IR detection) residual star formation activity. Among the emission-line galaxies, the star formation activity has declined with time in e(c) galaxies without a detectable burst, while in e(a) galaxies there is a mild-to-moderate burst of star formation at the OE.

The models are constrained to reproduce the FIR luminosity inferred from the mid-IR luminosity, not the SFR as indicated from the $24 \mu\text{m}$ measurements (section 4.3). Nevertheless, we find good agreement between what the modeling returns for the SFR over the time bin 2×10^7 yr and our “direct” determination of the SFR from the mid-IR. The agreement is not expected to be exact because (1) the FIR (from mid-IR) flux is one of many constraints in the models, and (2) the two paths incorporate different assumptions about the initial mass function and the timescales for the relevant calculations.

We summarize this section by noting that the star formation histories derived with the spectral modeling of star formation are consistent with the simple picture presented in Section 5 where we compared $24 \mu\text{m}$ and [O II] fluxes to distinguish the histories of galaxies of the different spectral classes. The results of this small, first study using Spitzer-MIPS data are consistent with the idea that e(a) and e(b) galaxies are active starbursts, k+a galaxies are the post-starburst phase of those galaxies, and e(c) galaxies are those that have not experienced any starbursts in the past few billion years. The numbers of cases and spectra are sufficiently small that we must consider this a preliminary step toward confirming the Poggianti et al. (1999) interpretation of galaxy spectra in intermediate-redshift clusters. For example, the e(a) galaxies studied here have a mass 2-3 times smaller than the two types of post-starbursts. This could easily be the result of the small sample sizes, but if it were to be confirmed with the much larger study we have begun, this would provide a puzzling distinction that would not fit with the simple model.

Cycle GO-4 observations of 27.5 hrs (PID 40387, PI A. Dressler) have been awarded to extend the coverage of Abell 851, and to observe two additional clusters at similar redshift, for which large spectroscopic samples of field and cluster galaxies have been obtained. These data should allow further investigation of obscured star formation in this cluster and its relevance to other intermediate-redshift galaxy populations.

8. Conclusions

Our study of optical spectroscopy and Spitzer-MIPS observations of a spectroscopic sample of cluster members of A851 at $z = 0.42$ has yielded the following results: (1) Detection with MIPS at $24 \mu\text{m}$ is a strong function of spectral type: almost all passive galaxies are undetected, and most normal starforming galaxies (type e(c), weak $\text{H}\delta$ absorption) are also undetected. However, some post-starburst galaxies (strong $\text{H}\delta$) and *most* e(a) galaxies (strong $\text{H}\delta$ and $[\text{O II}]$ emission) are detected. The non-detection of e(c) galaxies as compared to the detection of most e(a) galaxies occurs across the full range of luminosity sampled — in fact, the e(c)’s are systematically more massive in this sample — so this difference in detection is not a selection effect. (2) For the e(a) galaxies, the SFR derived from $24 \mu\text{m}$ is typically several times that inferred from $[\text{O II}]$, indicating a substantial amount of dust obscuration of ongoing star formation in these systems. Ongoing star formation is seen in some galaxies classified as post-starburst, for which $\text{SFR}(24 \mu\text{m})/\text{SFR}([\text{O II}])$ is likely to be as much as a factor of 10, but this it represents a significant decline from the burst that came before. (3) The high rates of star formation in e(a) galaxies — factors of 2-3 above the past average for these systems — qualifies them as moderate starbursts capable of accounting for the post-starbursts seen in A851, although for the specific, small samples we have here, there is a factor of 2–3 lower mass associated with the e(a) compared to the k+a galaxies. (4) A small sample of present-day starforming galaxies shows that these typically have $\text{SFR}(\text{IR})/\text{SFR}(\text{optical}) \sim 1$. We suggest that these galaxies are like the e(c) galaxies in A851, which would be consistent with these objects having $24 \mu\text{m}$ flux below the detection limit of these observations.

The assembly of these observations supports the model in which the e(a) galaxies and even some post-starburst galaxies are actually dust-obscured starbursts, with a factor of ~ 4 of the star formation hidden. As we will show in a forthcoming paper, the significant fraction of e(a) spectra among field galaxies at intermediate-redshift suggests that starbursts are also relatively common among field galaxies at intermediate-redshift. The rarity of such objects in the present-epoch universe indicates that star formation in ordinary spirals was more bursty — more variable — as recently as 4 Gyr ago. The extent and magnitude of this

phenomenon will become increasingly clear as further Spitzer-MIPS observations become available for intermediate-redshift clusters and the field.

9. Acknowledgments

The authors thank the referee for a careful review of the manuscript and many helpful suggestions. Dressler and Oemler acknowledge the support of the NSF grant AST-0407343. All the authors thank NASA for its support through NASA-JPL 1310394. Jane Rigby is supported by a Spitzer Space Telescope Postdoctoral Fellowship. Partial support was also provided through contract 1255094 from JPL/Caltech to the University of Arizona.

Table 1. Detection Rate of Spectral Types

Type	Total	Detected
k	41	2
e(c)	7	2
e(a) ^a	12	9
e(b)	3	1
k+a ^a	13	4
a+k	5	2
e(n)	2	2

^aAs explained in the text, two objects meeting the k+a criteria — $EW([O II]) > -5\text{\AA}$ and $EW(H\delta) > 3$ — but with detected [O II] are included in the e(a) rather than k+a numbers.

Table 2: Model summary.

	IR-det. k+a	Undet. k+a	e(c)	e(a)
N_{obj}	6	12	8	19
“all-time”	16 ± 3	12 ± 2	$7(7) \pm 3$	$3(3) \pm 0.8$
$6 \times 10^8 \text{yr}$	72 ± 7	$39(17) \pm 5(1)$	$1(2) \pm 2$	$6(7) \pm 2$
$2 \times 10^7 \text{yr}$	9 ± 1	1.1 ± 0.1	$1(2) \pm 1$	$7(7) \pm 3$
SFR($24 \mu\text{m}$)	12.1	<3.0	1.5	7.7
Mass	$1.5 \pm 0.3 \times 10^{11}$	$1.1 \pm 0.1 \times 10^{11}$	$7 \pm 0.6 \times 10^{10}$	$2.5 \pm 0.6 \times 10^{10}$

Note. — Average SFR ($M_{\odot} \text{yr}^{-1}$) per galaxy of each spectral class, as determined in the models. The SFR is averaged over the last 2×10^7 , 6×10^8 and over the age of the Universe at $z = 0.4$ — “all-time”, 9.2×10^9 yr. The values in parentheses come from adopting the $24 \mu\text{m}$ upper limit as opposed to the null value, in case of non-detection. The SFR($24 \mu\text{m}$) values, actual measurements, are to be compared to the 2×10^7 yr SFR from the model, as explained in the text. The last row contains the average galaxy stellar mass in solar masses.

REFERENCES

- Alonso-Herrero, A., Rieke, G. H., Rieke, M. J., Colina, L., Pérez-González, P. G., & Ryder, S. D. 2006, *ApJ*, 650, 835
- Bai, L., Marcillac, D., Rieke, G. H., Rieke, M. J., Tran, K-V. H., Hinz, J. L., Rudnick, G., Kelly, D. M., Blaylock, M., 2007, *ApJ*, 664, 181
- Balogh, M.L., Morris, S. L., Yee, H. K. C., Carlberg, R. G., & Ellingson, E., 1999, *ApJ*, 527, 54
- Brandl, B. R., et al. 2006, *ApJ*, 653, 1129
- Butcher, H., & Oemler, A. Jr., 1978, *ApJ*, 279, 18
- Calzetti, D., et al. 2007, *ApJ*, in press (astro-ph/0705.3377)
- Chary, R., & Elbaz, D. 2001, *ApJ*, 556, 562
- Couch, W. J., & Sharples, R. M., 1987, *MNRAS*, 229, 423
- Dale, D. A., & Helou, G. 2002, *ApJ*, 576, 159
- de Vaucouleurs, G., de Vaucouleurs, A., Corwin, H. G., Buta, R. J., Paturel, G., & Fouque, P., 1995, *Third Reference Catalog of Bright Galaxies (Revised)*, University of Texas Press.
- Dressler, A., & Gunn, J. E., 1983, *ApJ*, 270, 7.
- Dressler, A., Gunn, J. E., & Schneider, 1985, *ApJ* 294, 70
- Dressler, A., & Gunn, J. E., 1992, *ApJS*, 70, 1
- Dressler, A., Smail, I., Poggianti, B. M., Butcher, H., Couch, W. J., Ellis, R. S., & Oemler, A. Jr., 1999, *ApJS*, 122, 51
- Dressler, A., Oemler, A. Jr., Poggianti, B. M., Smail, I., Trager, S. C., Shectman, S. A., Ellis, R. S., & Couch, W. J. 2004, *ApJ*, 617, 867
- Duc, P.-A., Poggianti, B. M., Fadda, D., Elbaz, D., Flores, H., Chanical, P., Franceschini, A., Moorwood, A., & Cesarsky, C., 2002, *A&A*, 382, 60
- Egami, E. et al. 2006, *ApJ*, 647, 922

- Fritz, J., Poggianti, B. M., Bettoni, D., Cava, A., Couch, W. J., D’Onofrio, M., Dressler, A., Fasano, G., Kjrgaard, P., Moles, M., Varela, J., 2007, *A&A*, 470, 137
- Fadda, D., Elbaz, D., & Duc, P.-A., 2000, *A&A*, 382, 60
- Geach, J. E., Smail, I., Ellis, R. S., Moran, S. M., Smith, G. P., Treu, T., Kneib, J.-P., Edge, A. C., & Kodama, T., 2006, *ApJ*, 649, 661
- Gordon, K. D., Rieke, G. H., Engelbracht, C. W. et al. 2005, *PASP*, 117, 503
- Hunter, D. A., Gillett, F. C., Gallagher, J. S., III, Rice, W. L., & Low, F. J. 1986, *ApJ*, 303, 171
- Kennicutt, R. C., Jr. 1998, *ARA&A*, 36, 189
- Leitherer, C., Schaerer, D., Goldader, J. D., Delgado, R. M. G., Robert, C., Kune, D. F., de Mello, D. F., Devost, D., Heckman, T. M., 1999, *ApJS*, 123, 3
- Lilly, S. J., Eales, S. A., Gear, W. K. P., Hammer, F., Le Fvre, O., Crampton, D., Bond, J. R., & Dunne, L., 1999, *ApJ*, 518, 641
- Liu, C.T., & Kennicutt, R.C., 1995, *ApJ*, 450, 547
- Lonsdale Persson, C. J., & Helou, G. 1987, *ApJ*, 314, 513
- Marcillac, D., Rigby, J. R., Rieke, G. H., Kelly, D. M., 2007, *ApJ*, 654, 825.
- Marcillac, D., Elbaz, D., Chary, R. R., Dickinson, M., Galliano, F., & Morrison, G. 2006, *A&A*, 451, 57
- Matkovic, A. & Guzman, R., 2007, in “First Light Science with the GTC,” (Eds. R. Guzmán, C. Packham, J. M. Rodríguez-Espinosa, & S. Torres-Peimbert), *Revista Mexicana de Astronomia y Astrofisica (Serie de Conferencias)* Vol. 29, pp. 107-109
- Metcalfe, L., Fadda, D., & Biviano, A., 2005, *Space Science Reviews*, 119, 425 (arXiv:astro-ph/0506421)
- Moran, S. M., Ellis, R. S., Treu, T., Smith, G. P., Rich, R. M., Smail, I., 2007, arXiv:astro-ph/0707.4173
- Oemler, A., Dressler, A., Kelson, D., Rigby, J. Poggianti, B. M., Fritz, J., Morrison, G., & Smail, I., 2008, *ApJ*, submitted (Oem08)
- Poggianti, B. M., Smail, I., Dressler, A., Couch, W. J., Barger, A. J., Butcher, H., Ellis, R. S., & Oemler, A. Jr. 1999, *ApJ*, 518, 576 (P99)

- Poggianti, B. M., & Wu, H., 2000, *ApJ*, 529, 157
- Poggianti, B.M., Bressan, A., & Franceschini, A., 2001, *ApJ* 550, 195
- Prochaska, L. C., Rose, J. A., Caldwell, N., Castilho, B. V., Concannon, K., Harding, P., Morrison, H., & Schiavon, R. P., 2007, *AJ*, 134, 321
- , Rieke, G. H., Lebofsky, M. J., 1978, *ApJ*, 220, 37
- Rigby, J. R. et al. 2008, *ApJ*, submitted.
- Snchez-Blzquez, P., Peletier, R. F., Jimnez-Vicente, J., Cardiel, N., Cenarro, A. J., Falcn-Barroso, J., Gorgas, J., Selam, S., Vazdekis, A., 2006, *A&A*, 457, 823
- Schindler, S., Belloni, P., Ikebe, Y., Makoto, H., Wambsganss, J., & Tanaka, Y., 1998, *å*, 338, 843
- Smail, I., Morrison, G., Gray, M. E., Owen, F. N., Ivison, R. J., Kneib, J. -P., Ellis, R. S., 1999, *ApJ*, 525, 609
- Smith, J. D. T., Draine, B. T., Dale., D. A., et al., 2007, *ApJ*, 656, 770
- Tran, K.-V. H., Franx, M., Illingworth, G., Kelson, D. D., & van Dokkum, P. 2003, *ApJ*, 599, 865
- Treu, T., Ellis, R. S., Kneib, J.-P., Dressler, A., Smail, I., Czoske, O., Oemler, A., & Natara-jan, P., 2003, *ApJ*, 591, 53
- Wirth, G. D., Koo, D. C., Kron, R. G., 1994 *ApJ*, 435, 105